

# Numerical Prediction of Turbulent Combustion Flows in Staged Combustor Using LES and Extended G-Equation

Takuji TOMINAGA<sup>1</sup>, Yuichi ITOH<sup>2</sup>, Nobuyuki TANIGUCHI<sup>3</sup>, Toshio KOBAYASHI<sup>4</sup>,  
Tomoko HAGARI<sup>5</sup>, Yoshiharu NONAKA<sup>5</sup>

<sup>1</sup> School of Engineering, The University of Tokyo  
4-6-1 Komaba, Meguro-Ku, Tokyo 153-8505, JAPAN  
Phone: +81-3-5452-6198, FAX: +81-3-5452-6197,  
E-mail: tominaga@icebeer.iis.u-tokyo.ac.jp

<sup>2</sup> Institute of Industrial Science, The University of Tokyo

<sup>3</sup> Information Technology Center, The University of Tokyo

<sup>4</sup> Japan Automobile Research Institute    <sup>5</sup> Kawasaki Heavy Industry co. ltd

## ABSTRACT

In this study, the Large Eddy Simulation with the G-equation model is performed in the geometry of an axially staged annular combustor of a gas turbine engine. The propagation of flames in turbulent flow field depending on the equivalence ratios are represented by the extended G-equation model. The predicted results in the geometries of an experimental test piece and the modeled whole combustor are compared with each other, and are discussed using experimental data.

## INTRODUCTION

Numerical prediction of turbulent combustion in a gas turbine combustor is an important technology for designing and developing a gas turbine system, and, to realize an appropriate prediction, more accurate and effective simulations are expected.

For the reduction of harmful emissions such as NOx and CO, and for maintaining high efficiency of engine system, lean premixed combustion is one of key technologies in recent research of the gas turbine combustor. The lean premixed combustion, however, has some problems such as combustion oscillation or blow-out, especially in changing power settings. Those difficulties can be reduced by employing a staged combustor geometry and by controlling an output with a number of combustion areas.

For countering the difficulties in the lean premixed combustion, it is also important to understand the physics in a combustor. Turbulence effects, which often characterize the flow designs and affect to the flame propagation, should be calculated precisely. Large Eddy Simulation (LES), which needs no time-averaged modeling, is a suitable approach to analyze an unsteady turbulent flow field, while the G-equation approach

(Williams, 1985), in which chemical reactions are simplified by the flamelet assumption, can simulate premixed combustion phenomena with finite computer resources. These methods are also feasible to the practical prediction of combustion flows because the small scale phenomena, such as an effect of small vortices in the inertial range or an internal structure of flame, are generally modeled in the methods. Employing these approaches, a simulation methodology using a LES technique and the G-equation based on the flamelet concept was proposed (Menon, 1992) and has been evaluated (Park et al., 2001) for a simplified premixed combustion flow.

The objective of the present study is to validate the application of LES in the practical geometry of a gas turbine combustor and to simulate the flame propagation using G-equation model. The numerical simulations are performed in the geometry of experimental test piece sectors (Tsuru et al., 2002) of a whole annular combustor with/without a circumferential periodicity assumption. By comparing both the results with experimental data, some differences between the performances of the whole annular combustor and its cutout model are also discussed.

## NOMENCLATURE

$C_S$	Smagorinsky constant
$G$	Index scalar to represent flame surface
$p$	Pressure
$P$	$P = p/\rho$
$r$	Radial distance
$R$	Reference value of $r$
$s_L$	Laminar burning velocity
$s_T$	Turbulent burning velocity
$S_{ij}$	Strain rate tensor
$Sc$	Schmidt number
$Sc_{SGS}$	Turbulent Schmidt number
$t$	Time
$u_i$	Velocity in $i$ direction

$z$	Axial distance
$Z$	Reference value of $z$
$\delta$	Flame thickness
$\Delta$	Filter length scale
$\phi$	Equivalence ratio
$\phi_{main}$	$\phi$ of the gas from main nozzle
$\phi_{pilot}$	$\phi$ of the gas from pilot nozzle
$\mu$	Viscosity
$\mu_{SGS}$	Turbulent viscosity
$\theta$	Central angle
$\Theta$	Reference value of $\theta$
$\rho$	Density
$\sigma_G$	Parameter defining turbulent diffusion of $G$
$\tau_{ij}^{SGS}$	SGS stress tensor
$\xi$	Mixture fraction
$\tilde{f}$	Filtered value of variable $f$
$\bar{f}$	Favre Filtered value of $f$ ( $\bar{f} = \overline{\rho f / \rho}$ )

## NUMERICAL METHODS

In turbulent flows appearing in many industrial applications, combustion processes usually occur in a very small length and time scale compared to those of the turbulent flow field. According to the laminar flamelet concept (Menon, 1992), the flame can be assumed to have an infinitely thin structure comparing to the length scale of turbulent structures. Also, we can consider that a small parts of wrinkled flames in a turbulent flow, called 'flamelet', may have essentially the same characteristics as those of the laminar flame. Adopting these concepts, a turbulent premixed combustion can be described as the propagation and the convection of the filtered surface that separates burnt and unburnt gases on a LES grid system. The position of a flame surface is expressed by a contour surface of a scalar variable  $\bar{G}$  which depends on the spatially filtered G-equation (Menon, 1992). When a pair of premixed gases of different fuel equivalence ratios are mixed in the calculation domain, a non-uniform distribution of the equivalence ratios appears. To simulate the flame propagation in such a situation, the G-equation is coupled with a conserved scalar equation.

### Equations for Flow Field

The governing equations for LES of flow fields are written as follows:

$$\frac{\partial \bar{\rho} \tilde{u}_i}{\partial x_i} = 0 \quad (1)$$

$$\frac{\partial \bar{\rho} \tilde{u}_i}{\partial t} + \frac{\partial \bar{\rho} \tilde{u}_i \tilde{u}_j}{\partial x_j} = -\frac{\partial \bar{p}}{\partial x_i} + \frac{\partial}{\partial x_j} \left( \mu \frac{\partial \tilde{u}_i}{\partial x_j} - \tau_{ij}^{SGS} \right) \quad (2)$$

where  $\tau_{ij}^{SGS}$ , which is generated by the filtering operation, represents the SGS stress, and is represented by the Smagorinsky model (Smagorinsky, 1961) as,

$$\tau_{ij}^{SGS} \equiv \bar{\rho} (\tilde{u}_i \tilde{u}_j - \tilde{u}_i \tilde{u}_j) = -2\mu_{SGS} \tilde{S}_{ij} \quad (3)$$

$$\mu_{SGS} = \bar{\rho} (C_s \Delta)^2 |\tilde{S}| \quad (4)$$

where  $|\tilde{S}|$  is the square norm of  $\tilde{S}_{ij}$ . The model parameter  $C_s$  (called the Smagorinsky constant) is set to 0.1, which value is known to provide a good prediction of a parallel channel flow or a circular pipe flow.

### Equations for Flame Propagation

Following the laminar flamelet concept, the filtered G-equation for flame propagation is described as follows:

$$\frac{\partial \bar{\rho} \tilde{G}}{\partial t} + \frac{\partial \bar{\rho} \tilde{u}_j \tilde{G}}{\partial x_j} = \overline{\rho s_L |\nabla G|} + \frac{\partial}{\partial x_j} \bar{\rho} (\tilde{u}_j \tilde{G} - \tilde{u}_j \tilde{G}) \quad (5)$$

The index scalar  $\tilde{G}$  is assigned the value of zero in the unburned region and of unity in the burnt region with the thin flame identified by a fixed value of  $0 < G_0 < 1$ .

The first term on the right-hand side of eq.(5), which represents the flame propagation, is modeled using the turbulent burning velocity  $\bar{s}_T$  as follows:

$$\overline{\rho s_L |\nabla G|} = \bar{\rho} s_T |\nabla \tilde{G}| \quad (6)$$

$$s_T = \bar{s}_L \exp \left( \frac{u'^2}{s_T^2} \right) \quad (7)$$

$$u' = C_t \Delta |\tilde{S}| \quad (8)$$

where eq.(7) for the evaluation of  $s_T$  is a model equation proposed by Yakhot (Yakhot, 1988), and  $u'$  is the turbulent velocity fluctuation determined by eq.(8). Based on the assumption of  $C_s = 0.1$  and the dimension analysis under an isotropic-turbulence condition, the parameter  $C_t$  is determined to be 0.15.

The second term on the right-hand side of eq.(5) can be modeled as a SGS turbulent flux. Assuming a linear diffusion, it is evaluated as

$$\bar{\rho} (\tilde{u}_j \tilde{G} - \tilde{u}_j \tilde{G}) = -\frac{\mu_{SGS}}{\sigma_G} \frac{\partial \tilde{G}}{\partial x_j} \quad (9)$$

This term acts to eliminate cusps of the scalar  $G$ . The coefficient  $\sigma_G$  appearing in this equation represents the diffusion intensity of  $G$ , and is set to 0.25 (Smith and Menon, 1994).

To close the system of equations for premixed combustion flows, we need a way to determine the local burning velocity  $\bar{s}_L$  which depends on the mixture fraction  $\tilde{\xi}$ . The conservation equation for the mixture fraction  $\tilde{\xi}$  is described as follows:

$$\frac{\partial \bar{\rho} \tilde{\xi}}{\partial t} + \frac{\partial \bar{\rho} \tilde{u}_j \tilde{\xi}}{\partial x_j} = \frac{\partial}{\partial x_j} \left\{ \left( \frac{\mu}{S_c} + \frac{\mu_{SGS}}{S_c S_{SGS}} \right) \frac{\partial \tilde{\xi}}{\partial x_j} \right\} \quad (10)$$

For the translation from  $\xi$  to  $s_L$ , the approximation equation proposed by Götting et al. (Götting et al., 1992) is adopted. This equation was given theoretically, and the parameters in this are fitted to numerical data. Using the approximation equation and the spatial distribution of the equivalence ratio given by Eq.(10),  $\bar{s}_L$  is determined.

Additionally, the flame extinction affected by flame stretching is modeled as follows. Following Inage's model (Inage and Ohtsuka, 1997), we assume the burning velocity to be zero in the condition of

$$|\tilde{S}| \frac{\delta}{s_L} > Ka_q \quad (11)$$

where  $Ka_q$  is a parameter like a Karlovitz number when the extinction occurs. In the present calculation,  $Ka_q$

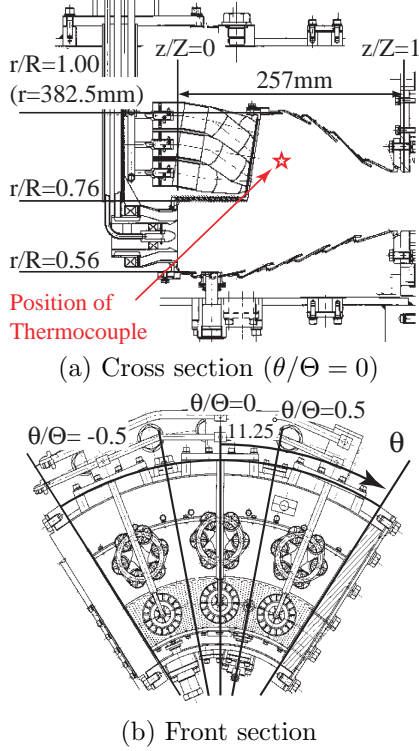


Fig.1: Schematic figures of the model combustor

is set to 5.0. The flame thickness  $\delta$  is evaluated by an approximated equation based on a theoretical analysis and numerical data (Göttgens et al.,1992).

In this study, the calculations are performed using the incompressible assumption in both non-combustion and combustion cases. In the combustion turbulent flow field, a dilatation of a mixture gas caused by a combustion reaction should accelerate a burnt gas and change a flow field. Then the use of incompressible assumption and a neglect of this effect may cause quantitative errors in a prediction of combustion flow. Although an increase of viscosity caused by a high temperature also should effect to the flow field, its effect may small in this case because the turbulent viscosity is dominant in such a highly turbulent flow.

## MODEL COMBUSTOR AND NUMERICAL CONDITION

The geometry of the model combustor built for an experimental study and assumed in the present study is shown in Figure 1 (Tsuru et al., 2002). This test piece is a 3-sector cutout model of a typical staged annular combustor that has 16 sectors in total. Pilot flame exists in the inner pilot stage, which propagates to the outer main stage when a higher power is needed. The pilot nozzle has a double-swirler to generate the recirculation region and to hold pilot flame. The main nozzle consists of 6 twisting tubes in which the fuel and air are premixed. To protect the liner wall from hot burnt gases, a film-cooling method is used to cool it out. In the experiment, Methane gas is chosen as fuel, since there are many difficulties in the prediction of combustion with liquid fuel spray. The premixed gas is pre-heated to 623[K] in the experiment of combustion flow.

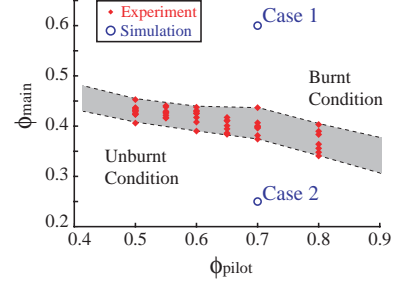


Fig.2: The equivalence ratio when the flame propagation observed in experiments (Tsuru et al., 2002) (The plots of “simulation” mean the condition in which the numerical simulation is demonstrated. The plots of “Experiment” mean the igniting  $\phi_{main}$  values in the several trials with each of  $\phi_{pilot}$  values. )

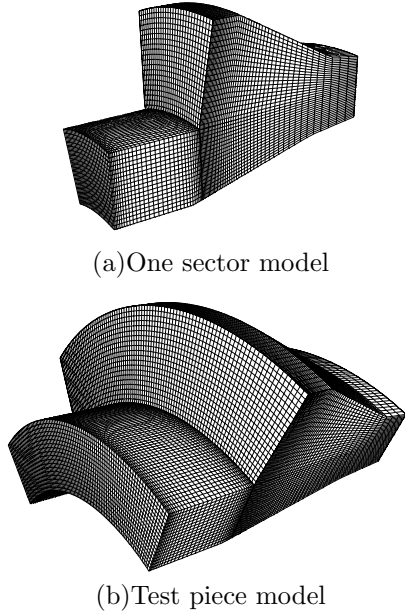
## Experimental Data

In the experiment of non-combustion flow, the velocity distribution is obtained using a hot-wire anemometry. The X-type probe is used to measure the axial and the circumferential velocity components simultaneously.  $z$ ,  $r$ , and  $\theta$  shown in Figure 1 are the axial, radial and circumferential coordinates, respectively. These are non-dimensionalized by  $Z = 257$  mm (the total length of the liner),  $R = 382.5$  mm (the maximum radius of the outer liner), and  $\Theta = 22.5$  degree (the center angle of a sector), respectively.

In order to investigate the limitation of the flame propagation from the pilot stage to the main stage, the equivalence ratio at the exit of the main nozzle  $\phi_{main}$  is measured when the flame propagation occurs. Procedure of the measurement of  $\phi_{main}$  is as follows: firstly, a certain amount of fuel is supplied only to the pilot nozzle, and then, when a stable flame is formed in the pilot stage, fuel supply to the main nozzles is started and its amount is gradually increased to propagate the flame to the main stage. When the flame propagates, the amount of fuel supplied to the main fuel nozzles is measured and  $\phi_{main}$  is determined. The flame propagation observed by a sudden temperature rise more than 300 K is detected by a thermocouple located close to the exit of the main nozzles (Figure 1). This procedure is carried out several times for each value of  $\phi_{pilot}$ , which represents an equivalence ratio at the exit of the pilot nozzle. The results are shown in Figure 2. Some differences can be observed in the value of  $\phi_{main}$  for different examinations under the same condition.

## Computational Model

In the present study, two types of computational domain are defined for simulation. The grid systems of the two different domains are shown in Fig.3. The first domain is a single sector of the combustor (called “One-sector model” in this paper). Assuming the circumferential periodic boundary condition, the calculation can simulate approximately a whole annular combustor geometry, although phenomena appearing in the true multi-sector cannot be observed. The second domain (called “Test piece model”) has three sectors of the combustor, the same as the experimental test piece



(a)One sector model

(b)Test piece model

Fig.3: Computational grid system  
(The half of the grids are thinned out in each direction.)

Table 1: Computational conditions

Reynolds Number		59600
Pressure (MPa)		0.1013
Temperature (K)		623
Fuel		Methane
Equivalence ratio	$\phi_{main}$	0.25, 0.6
	$\phi_{pilot}$	0.7

mentioned above. The free-slip boundary condition is adopted to the circumferential boundaries. These two models are different in size, but have the same grid resolution. The grid resolutions in each direction are  $\Delta z = 0.00197Z \sim 0.021Z$ ,  $\Delta r = 0.00564R$ , and  $\Delta\theta = 0.0167\Theta$ , respectively. These grid widths in  $r$  and  $\theta$  directions correspond with about thirtieth part of the pilot nozzle diameter. The numbers of grids are approximately 590,000 in “One-sector model” and 1,770,000 in “Test piece model”.

The other boundary conditions for the present calculations are as follows. The inlet velocity distribution from the pilot nozzle is determined using experimental results obtained by a stereo-PIV system at the exit of the nozzle. The inlet velocity distribution from the main nozzle is assumed to be uniform on the exit of the nozzle. The airflow entering through the cooling slot is modeled by the free-slip condition on the liner wall boundary. The convective boundary condition is adopted for the outlet boundary condition.

The computational conditions listed in Table 1 are chosen to be the same as the physical conditions of the referenced experiment except for the equivalence ratio. The fuel equivalence ratios for the simulations of flame propagation are fixed in the two cases represented.

### Computational Methods

In the calculation, the governing equations are

Table 2: Computational methods

Methods for Filtered N-S equation (Kogaki(1999))	
Coupling algorithm	Fractional step method ( $\Delta t = 2.0 \times 10^{-6}$ [sec])
SGS model	Smagorinsky model
Spatial differential scheme	Second-order central differential scheme
Time advancing scheme (advection term)	Second-order Adams-Bashforth scheme
(diffusion term)	Crank-Nicolson scheme
Stabilizing method	6th-order explicit filter
Method for Scalar transport equations ( $G$ and $\xi$ )	
Spatial differential scheme (advection term)	QUICK scheme
(diffusion term)	Second-order central differential scheme
Time advancing scheme	Second-order Adams-Bashforth scheme

spatially discretized based on the LES code with a Boundary Fitted Coordinate (BFC) scheme (Kogaki et al., 1999). The other computational methods are listed in Table 2. The computations are conducted by an in-house parallel code.

## RESULTS AND DISCUSSION

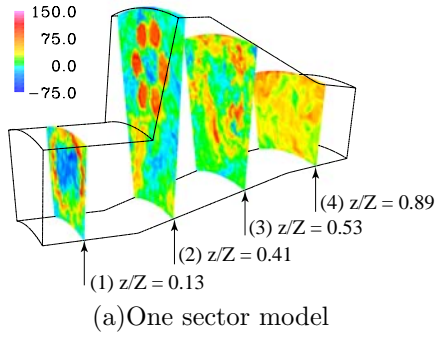
### Non-combustion Turbulent Flow

Firstly the non-combustion turbulent flow field in the combustor is calculated by LES. The contours of an instantaneous axial velocity are shown in Figure 4.

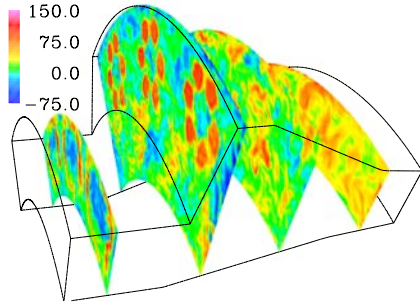
A difference between the results for the two models appears in a secondary flow. In the one-sector model with the periodic boundary condition, a circumferential flow around the whole annular combustor is predicted. However, in the test piece model such a flow is prevented by the side walls, and a clockwise flow around the domain is predicted. This difference can be observed clearly in Figure 5. In this figure, the circumferential velocities in the inner (down-side) region have the opposite directions in each model. Near the side walls of the test piece model, the flow from outer to inner on the right side and one from inner to outer on the left side are predicted.

Figures 6, 7, 8, and 9 display the profiles of the axial and the circumferential time-averaged velocities on the centerline ( $\theta/\Theta = 0$ ) of the planes (1) and (2) shown in Figure 4. Also, the experimental data is also plotted in these graphs.

In the pilot stage, the re-circulation region generated by the strong swirl is predicted as a negative value of an axial velocity (Figure 6) with a gradient of circumferential velocity (Figure 7) on plane(1) ( $z/Z \approx 0.13$ ). The axial velocity profile predicted in the test piece model is in agreement with the experimental data, though the predicted peak values are larger by 25% than the measured values. The profile predicted for the one-sector model is also in agreement with the profile in the test piece model, while the positive peaks in the inner side

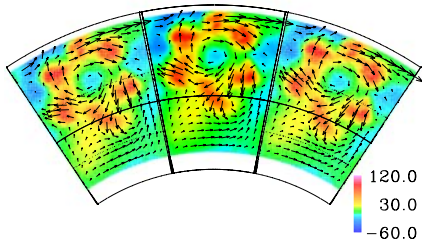


(a) One sector model

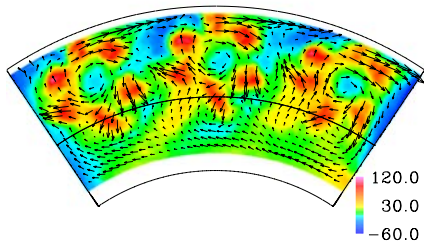


(b) Test piece model

Fig.4: Contour plot of instantaneous axial velocity



(a) One Sector Model with Periodic Boundary



(b) Test Piece Model

Fig.5: Averaged velocity distribution on the center of plane at  $z/Z = 0.65$

( $r/R = 0.57 - 0.6$ ) for the different models have different positions from each other. For the circumferential velocity (Figure 7), the curves predicted in the two models have similar tendency with each other. However, in the one-sector model, the curve shifts toward a higher velocity range from one predicted in the test piece model. In the one-sector model, the direction of swirling flow structure from the pilot nozzle is changed by the flow around the whole annular combustor in the circumferential direction. On the other hand, in the test piece model, the circumferential flow and also the movement of the structure are prevented by the side-walls. This

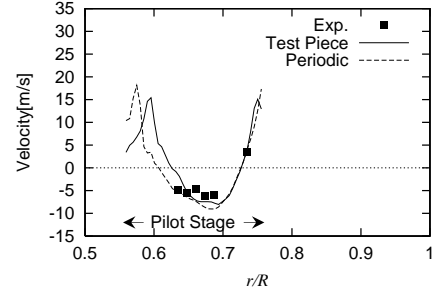


Fig.6: Comparison of the axial velocity at the center of plane(1)

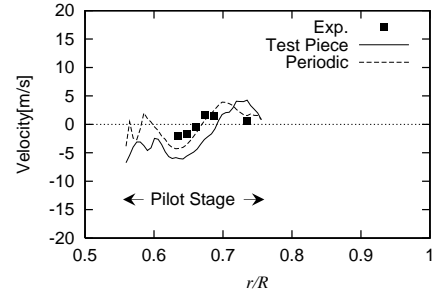


Fig.7: Comparison of the circumferential velocity at the center of plane(1)

difference results in the shift of the curve in Figure 7. In spite of these discrepancies, the predicted value in the one-sector model without the side walls is even close to the experimental data rather than the value in the test piece model. This result indicates that the test piece model calculation over-estimates the side-wall effect. It is suspected that the distribution of the cooling-air flow rate could become too uneven in the circumferential direction to decrease the side-wall effect, because the flow prevented by the side walls causes the pressure gradient in the circumferential direction. In the present calculation, the uneven distribution of the cooling-air flow rate is not considered, because the cooling-air flow is modeled by the free-slip boundary. Thus, the modeled boundary condition might be a cause of the over-estimation.

The re-circulation region and swirling flow are predicted also in the plane (2) ( $z/Z \approx 0.41$ ). The experimental data indicates that the axial velocity becomes positive on plane(2) and thus the size of the re-circulation region is over-estimated in the simulation. It is suspected as the reason of the above errors that the turbulent diffusion is under-estimated by neglecting the fluctuation in the inlet boundary. Near the inner walls ( $r/R = 0.58 - 0.67$ ), the negative circumferential velocity is predicted in the test piece model because of the affect of the flow around the test piece, while such a profile is not predicted in the one-sector model. The same situation exists in the region near the outer wall ( $r/R = 0.96 - 1.0$ ) in the main stage, where the circumferential velocity in the test piece model becomes greater than in the one-sector model.

In the main stage, the essential flow structure predicted in each model are in agreement with each other. Furthermore, the effects of the side-walls appear only

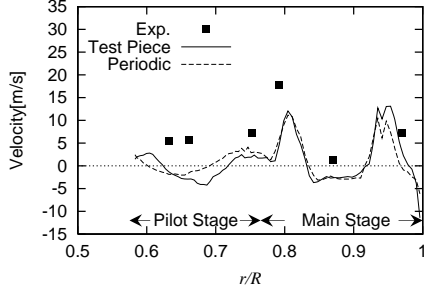


Fig.8: Comparison of the axial velocity at the center of plane(2)

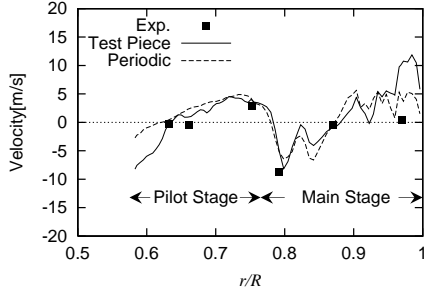


Fig.9: Comparison of the circumferential velocity at the center of plane(2)

near the outer wall. The experimental data at  $r/R = 0.79$  and  $0.97$  are located in the jets from the upper and lower tubes, respectively, and the data at  $r/R = 0.87$  is located at the center of the jets. The peaks of the predicted axial velocity cannot be evaluated, because the number of the measured points is not enough. According to the predicted axial velocity distribution in the plane (2), the discrete jets do not run through the center of the plane ( $\theta/\Theta = 0$  shown in figure 8). Meanwhile, the velocity on the edge of the jets is shown as a predicted peak velocity in Figure 8, therefore a difference in the direction of the jets may strongly affect the magnitude of the velocity. This may be the reason of the different axial velocities between the simulation profile and the experimental data in the jets. The re-circulation region at the center of the jets is not observed clearly in the experimental data, while it has been predicted numerically for  $r/R = 0.84 \sim 0.92$  and the swirl flow also predicted in the same position in the simulation. It may be the over-estimation of the re-circular region just like in the case of the pilot stage, because the time-averaged inlet condition is used for the main nozzle.

### Flame Propagation

As an objective of the present calculation for combustion flows, the flame propagation from the pilot stage to the main stage is chosen. The fully developed turbulent flow field mentioned above is used for the initial condition.

**Mixture Fraction.** The mixture fraction  $\bar{\xi}$  represents the gases from the pilot nozzle and from the main nozzle with the values of  $\bar{\xi} = 1$  and  $0$ , respectively. For the initial distribution of  $\bar{\xi}$ , the preliminary calculation of the  $\bar{\xi}$ -equation with a turbulent flow field is executed

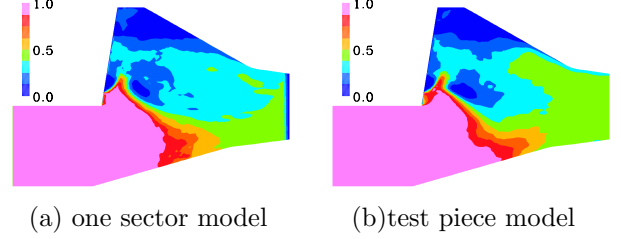


Fig.10: Time averaged distribution of mixture fraction  $\bar{\xi}$  on plane  $\theta/\Theta = 0.0$

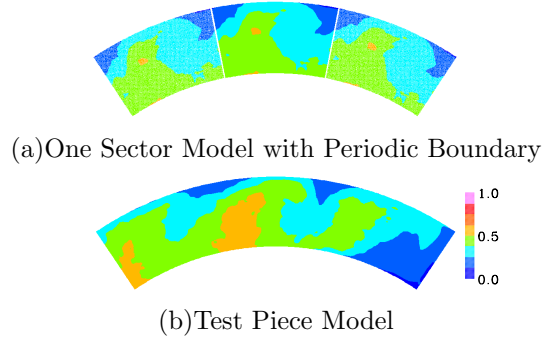


Fig.11: Time averaged distribution of mixture fraction  $\bar{\xi}$  on plane (4)

until the time-average of  $\bar{\xi}$  converges.

The time-averaged  $\bar{\xi}$  distributions on a plane  $\theta/\Theta = 0.0$  are shown in Figure 10. The pilot region is filled with the gas from the pilot nozzle, which is represented by  $\xi = 1$  in each model. Comparing the results for the two models, the affect of different flow fields is clearly shown as a difference of the  $\bar{\xi}$  distribution near the inner (lower) wall. The predicted value of  $\bar{\xi}$  in the test piece model is higher than that in the one-sector model. Near the outlet of the combustor, the value of  $\bar{\xi}$  in test piece model is slightly higher than that in the one-sector model. The time-averaged  $\bar{\xi}$  distributions on plane (4) ( $z/Z = 0.89$ ) near the outlet are also shown in Figure 11. In the side sectors of the test piece model, not only the value of  $\bar{\xi}$  but also its distribution are different from the results for the one-sector model. However, the profile of  $\bar{\xi}$  in the central sector of the test piece model corresponds to the profile in the one-sector model, though the values are slightly different. In the same figure, we can observe that an uneven distribution is affected by the flow around the test piece mentioned above. The predicted clockwise flow around the test piece takes the main gas from the outer region (upper region) to the right side and it also takes the pilot gas to the left side. The  $\bar{\xi}$  distribution should affect the results of the G-equation calculation for flame propagation, because it determines the local burning velocity in the G-equation calculation.

**Flame Propagation.** The preliminary calculation for obtaining the initial distribution of  $\bar{G}$  is carried out as follows: the G-equation with the fixed flow field and the fixed  $\bar{\xi}$  distribution is advanced in the condition of  $\phi_{main} = 0.0$ ,  $\phi_{pilot} = 0.7$  until the calculation converges, where  $\phi_{main}$  and  $\phi_{pilot}$  indicate the gases from the pilot

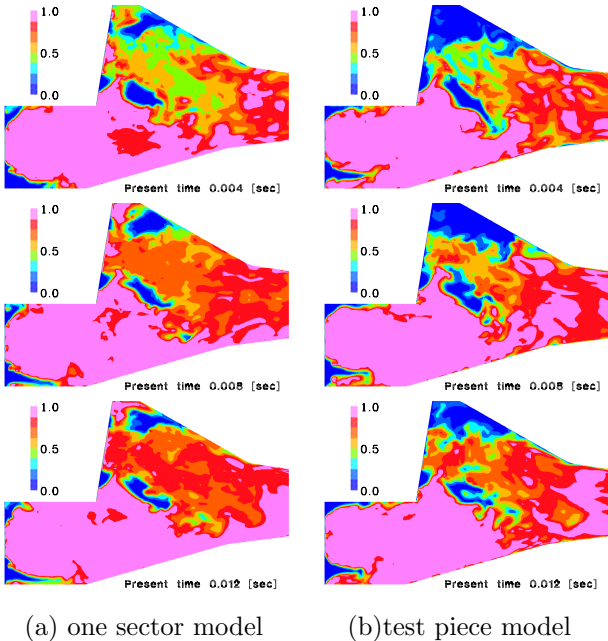


Fig.12: Time evolution of flame (contour of scalar  $G$ ) in case 1 ( $\phi_{main} = 0.6, \phi_{pilot} = 0.7$ )

nozzle and from the main nozzle, respectively, and an ignition point ( $\bar{G} = 1.0$ ) is set in the re-circulation region of the pilot stage. Starting from this initial condition, the calculations of the G-equation are conducted in two cases of the fuel equivalence ratio plotted in Figure 2. The experimental results reveal that the flame propagation from the pilot region to the main region does not occur in the case of  $\phi_{main} = 0.25$  and  $\phi_{pilot} = 0.7$  (Case 2), but occurs in the case of  $\phi_{main} = 0.6$  and  $\phi_{pilot} = 0.7$  (Case 1).

In Figures 12 and 13, the time evolutions of the scalar  $G$  on the central surface of the sector are illustrated from top to bottom at every 4ms after the simulations start. The flames propagate to the main stage through two pathways. In one way, a flame propagates back from the downstream along the centerline of the main nozzle. In the other way, a flame propagates radially around the jets from the main nozzle, and it comes into the center of the main nozzle outlet through between the jets. Then, it holds in the re-circulation region of the main region.

In the case 1, the flame from the downstream joins with one held in the re-circulation region and spreads to the whole sector stably. On the other hand, in the case 2, the burnt gas from the downstream reaches the re-circulation region in the main stage, however, the burnt gas has a place intermittently in the main stage, because the flame is unstable. We consider that the results in case 2 correspond to the experimental feature in the shaded area of Figure 2. Then, in this simulation the lean limit of for the flame propagation to the main region is predicted leaner than the observed limitation in the experiments. In the case 2, the  $\bar{G}$  distribution is not steep in the center of the six main jets, where the local burning velocity is slow compared to the turbulent velocity fluctuation. It is suspected that, in this region,

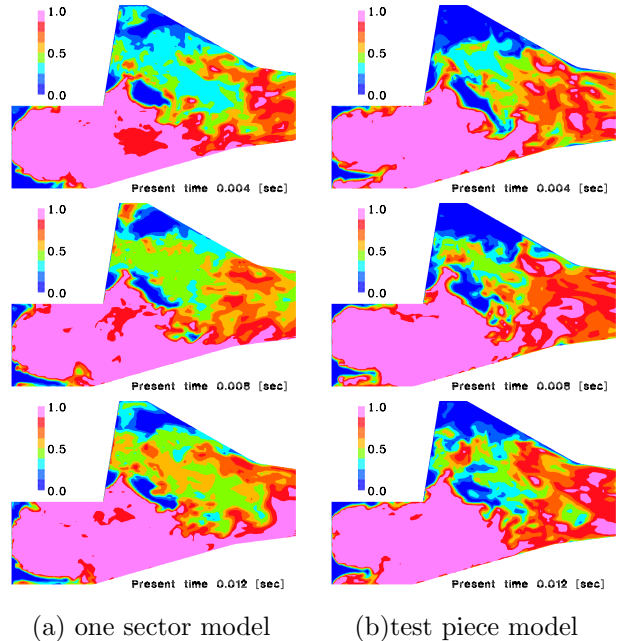


Fig.13: Time evolution of flame (contour of scalar  $G$ ) in case 2 ( $\phi_{main} = 0.25, \phi_{pilot} = 0.7$ )

the  $\bar{G}$  distribution rather represents the mixture of the burnt and the unburnt gases than the thin flame propagation. To predict the limit for the flame propagation with a better accuracy, the G-equation model should be extended into such a condition.

These typical flame behaviors can be observed in one-sector model and in the central sector of the test piece model, while these flame behaviors have little differences in each model because of the differences in the flow fields and in the  $\bar{\xi}$  distributions. Near the outer wall, the flame propagation has been predicted only in the one-sector model. This difference is caused by the difference of  $\bar{\xi}$  distribution in the pathway of the flame propagation. However, considering that the results are instantaneous data taken from different instantaneous  $\bar{G}$  distributions, we can consider that the flame behavior is not so different at the position of thermocouple in the experiment. Furthermore, these results indicate that the limitation of flame propagation is not affected by the existence of the side walls in the test piece. Figure 14 shows the flame surfaces 0.012 second after the start of calculations in the test piece model. On the outlet surface, a larger amount of the burnt gas exists in the left sector than in the right sector. This uneven distribution of burnt gas in the side sectors of the test piece model is caused by the distribution of the gas from the pilot nozzle predicted by the equation of the mixture fraction  $\bar{\xi}$ , because the pilot gas has a higher equivalence ratio than that of the gas inflowing from the main nozzle.

## CONCLUSION AND PROSPECTS

The LES incorporating the G-equation model based on the flamelet assumption has been demonstrated to predict the unsteady turbulent flow and the flame propagation in a practical combustor geometry. This sim-

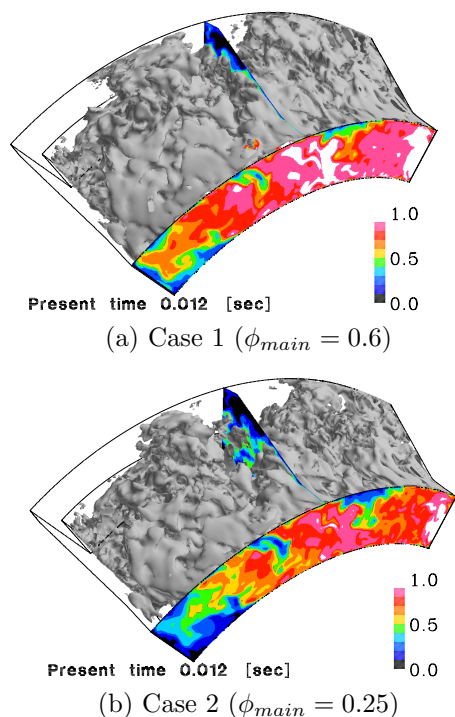


Fig.14: Predicted flame surface (gray surface) and contour of scalar  $G$  in Case 2

ulation employing the extended model can predict the following essential characteristics to design the annular staged combustor:

1. The gas from the pilot nozzle fills the pilot stage completely in any cases, and the equivalence ratio of the main nozzle does not affect the flame behavior in the pilot stage.
2. The difference of the flame behaviors in the main stage is predicted for various equivalence ratio as observed in the experiment. However, the limit for the flame propagation toward the main stage is predicted to be leaner than the experimental data.

To predict a flame propagation with a better accuracy, the improvement of the flamelet model is needed in the region where the local burning velocity becomes slow compared to the turbulent fluctuation velocity just like the center of the six main jets.

The comparisons of the results in the two different computational domains suggest that:

1. in the test piece model with the side-wall boundaries, the existence of the walls generate the flow around the periphery of the test piece. This flow has however been overestimated. The boundary conditions on the walls should be refined more realistic for a precise estimation of the affect.
2. in the central sector, the results for the mixture fluctuation distribution and flame propagation are not so different from the predicted results in the one-sector model except near the exit of the main region.

The turbulent velocity field predicted by LES is also compared with the experimental data. To achieve accurate prediction of the re-circulating and swirling flow, further investigations concerning the appropriate velocity fluctuation in the inlet boundary condition are needed.

## ACKNOWLEDGMENT

This study was supported by Frontier Simulation Software for Industrial Science under an IT program of MEXT. All Computations have been performed by HITACHI SR8000/MPP and SR8000/128 in Computer Center, the University of Tokyo.

## References

- Smagorinsky, J., "general circulation experiments with primitive equations", *Monthly Weather Rev.* 91-3, pp.99-164, 1963
- Williams, F. A., *Combustion Theory* (2nd ed.), Addison-Wesley, 1985
- Smith, T.M. and Menon, S., "The Structure of Constant Property Propagating Surfaces in a Spatially Evolving Turbulent Flow", 25th AIAA Fluid Dynamics Conference, 1994.
- Menon, S., "Active Combustion Control in a Ramjet Using Large-Eddy Simulations" *Combustion Science and Technology*, vol.84 pp.51-79, 1992
- Müller, U. C., Bollig, M., and Peters, N., "Approximations for Burning Velocities and Markstein Numbers for Lean Hydrocarbon and Methanol Flames", *Combustion and Flames*, Vol. 108, pp. 349-356, 1997.
- Park, N., Kobayashi, T., and Taniguchi, N., "Application of Dynamic Subgrid G-Equation Model to LES of Turbulent Premixed Flame over Backward Facing Step", *Proceedings of Turbulence and Shear Flow Phenomena 3*, 2001
- Kogaki, T., Kobayashi, T., and Taniguchi, N., "Conservative finite difference Schemes for Incompressible Turbulent Flow in Generalized Coordinates", *Proceedings of Turbulence and Shear Flow Phenomena 1*, 1999
- Inage, S., Ohtsuka, M., *Transactions of JSME*, 63-609, B(1997), pp. 1806-1813 (in Japanese)
- Göttgens, J. et al., "Analytic approximations of burning velocities and flame thicknesses of lean hydrogen, methane, ethylene, ethane, acetylene, and propane flames" *Twenty-Fourth Symposium (International) on Combustion/The Combustion Institute*, pp.129-135, 1992
- Yakhot, V., "Propagation Velocity of Premixed Turbulent Flames", *Combustion Science and Technology*, Vol. 60, 1988
- Tsuru, T., Imamura, A., Kinoshita, Y., Nonaka, Y., Itoh, Y., Taniguchi, N., "Numerical Simulation of Flame Propagation in a Staged Combustor" *Proceedings of ASME Turbo Expo 2002*, June 3-6, 2002, Amsterdam, The Netherlands